# Supplementary Information for "Agile reversible shape-morphing of particle rafts"

by Kyungmin Son, Jeong-Yun Sun, and Ho-Young Kim

## 1. The maximum response speed and the effective viscosity of upheaved particle raft

The tall mound of particle aggregate is elongated as the top electrode is raised at a speed below the critical speed $U_c$. The effective viscosity of the upheaved particle raft $\mu_e$ can be estimated from $U_c$. The equation of motion of a mass-spring-damper system with mass $m$, damping coefficient $b$, spring constant $k$, and displacement $z$ is given by $m\ddot{z} + b\dot{z} + kz = 0$ with the overdot denoting the time derivative. In our particle raft system, $b \sim \mu_e L$ and $k \sim \gamma_p$, where $L$ is the characteristic height of the upheaved raft. Assuming $L \approx 3$ mm and the characteristic response time $\tau \approx 0.5$ s from Fig. 3(a) and (c) in main text, respectively, the inertia term is scaled as $m\ddot{z} \sim \rho L^3 Z/\tau^2 \sim 10^{-4} Z$ kg m/s$^2$ with $Z$ the scale of $z$. Because the inertia term is negligible compared with the surface tension term $\gamma_p z \sim 10^{-2} Z$ kg m/s$^2$ ($\gamma_p$ is measured to be 30.2 mN/m), the dynamics of highly damped particle raft leads to $\mu_e L Z/\tau \sim \gamma_p Z$. Thus, the effective viscosity is scaled as $\mu_e \sim \gamma_p \tau/L \sim \gamma_p/U_c$. Substituting $\gamma_p \approx 0.03$ N/m and $U_c \approx 4$ m/s (Fig. 3(c) in main text), $\mu_e$ is estimated to be 7.5 Pa·s, which lies between the viscosities of castor oil $\mu_c$ and wet particle assembly composed of hollow glass particles and castor oil $\mu_p$ (Fig. S1).

## 2. Reversible height change of raft tower

The particle raft grown by the remote pulling returns to the flat interface when the potential difference is eliminated. Because the final electrode distance is larger than the initial distance, applying potential again only slightly deforms the raft due to the weakened field. However, if electric potential is applied before the raft descends to a critical height, the electrostatic force is sufficient to raise the raft back to the original height. Therefore, the reversible height change is possible by adjusting the potential difference in the height range of raft where the electrostatic force can be stronger than the resisting force (Fig. S2).

### 3. Effects of the electrode diameter on the width of the upheaved particle raft

Because the diameter of the electrode affects the shape of the electric field, we can expect the shape of the upheaved raft to vary depending on the diameter of the electrode. We fixed the height of the electrode and observed the change in width of the upheaved raft $w$ by varying the diameter of the electrode $d$ (Fig. S3(a)). The deformation of raft for electrodes with $d$ ranging from 10 to 25 mm at $h = 3.8$ mm is shown in Fig. S3(b). As $d$ increases, the upheaved mound gets wider. This is because the larger the electrode diameter, the wider the high voltage region and the greater the electrostatic force acting on the interface. The width of the upheaved raft is plotted versus $d$ in Fig. S3(c), indicating that $w$ increases with $d$ and tends to saturate near $d = 25$ mm. This saturation comes from the fact that the electric field becomes uniform as $d$ increases, so that the electrostatic force acting on the upheaved interface becomes independent of the electrode size.

### 4. Leakage current at exceedingly high electric potential

When an excessively high voltage is applied to the particle raft system under atmospheric conditions, a strong electric discharge occurs due to a strong electric field around the top electrode (Fig. S4(a)). The current flowing through the top electrode has been measured via a current meter when $h$ is fixed at 7 mm. As shown in Fig. S4(b), the current increases rapidly as $\phi$ increases beyond 7 kV. The large leakage current not only perturbs the interface under the electrode (Fig. S4(c)), but also weakens the electrostatic force, thereby inhibiting stable upheaval of the raft. According to the experiments with $d = 10$ mm and $h = 7$ mm, the interface becomes unstable exhibiting ripples with no stably upheaved mound when $\phi$ exceeds 12 kV.

**5. Suppression of discharge at high potential difference through gas substitution**

Upheaving a raft from an electrode far from the unperturbed surface is advantageous for increasing the mound height. However, a large electric potential is required to this aim because the electric field acting on the raft by the distant top electrode must be large enough to deform the interface. Therefore, leakage current must be prevented in order to deform the interface without undesired perturbations even at large red electric potential.

It is the pressure and type of the gas that determine whether the electric discharge occurs. To prevent discharge around the electrode, we tested an insulating gas, sulfur hexafluoride ($SF_6$), which has good discharge and arc quenching property [1]. We set up the particle raft system inside a gas chamber, replaced the interior air with $SF_6$, and applied electric potential difference (Fig. S5(a)). In the chamber at 1 bar of 10 vol.% air and 90 vol.% $SF_6$, the upheaved

raft with $h = 10.5$ mm and $\phi = 21.5$ kV is shown in Fig. S5(b). Compared with the raft in the atmospheric condition shown in Fig. S5(c), a larger deformation was achieved at a higher elevation of the top electrode in the $SF_6$-rich environment. The regime boundary where strong uplift of the raft occurs (as a green boundary in Fig. 2(c) in main text) in $SF_6$-rich environment is also in good agreement with our approximate model, $\phi \sim (\rho g/\Delta\epsilon)^{1/2} h^{3/2}$ (Fig. S5(d)). This reveals the capability of our electro-morphing scheme to form objects of a fairly high aspect ratio using insulating gases at high pressure.

**6. Three-dimensional physical display using transparent electrodes**

The capability of the particle raft to upheave without any pre-defined patterns allows us to envision one of its applications as a time-varying 3D physical display sculpted by the electric field. Fig. S6 exemplifies such a device, where each pixel of transparent ITO (indium tin oxide) electrode establishes its own electric field to locally deform the particle raft where desired. Fig. S6(c) and (d) show the 3D letters, SNU, that have been formed by turning the electrodes selectively (Movie S3). The device can erase the letters by turning the electrodes off and generate different 3D patterns anew. The rising height of individual pixels can be controlled by adjusting the electric potential or height of each electrode, as delineated above.

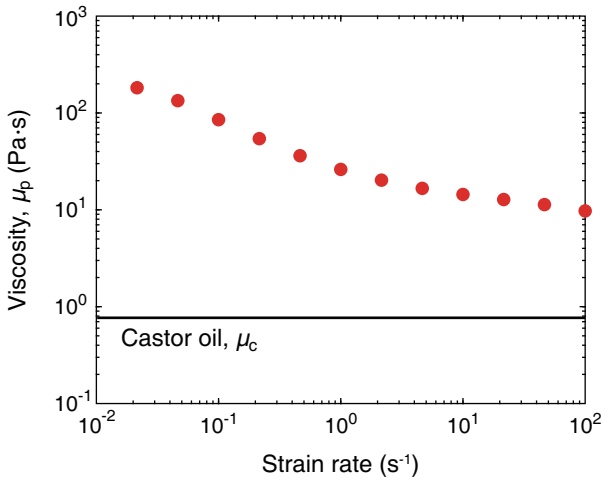


FIG. S1: Viscosity of wet particle assembly. The viscosity of the wet particle assembly composed of hollow glass particles and castor oil with the volume ratio of 1:1. Viscosity decreases with strain rate, exhibiting a shear-thinning behaviour.

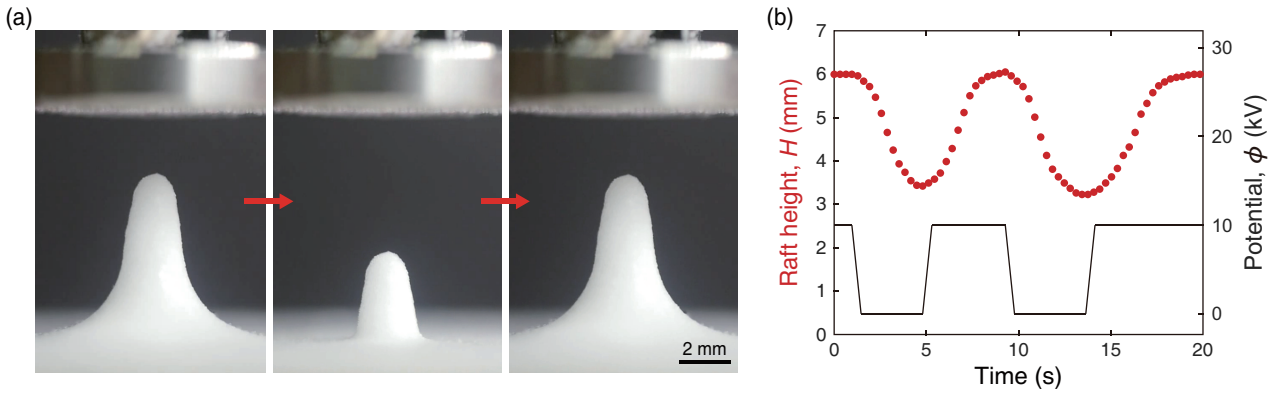


FIG. S2: Particle aggregate that reversibly changes in height by varying potential difference. (a) The elongated particle aggregate descends when the potential difference is eliminated. If the potential difference is increased again before the particle aggregate falls below a critical height, the aggregate rises again. (b) Height change of particle aggregate with the time-varying electric potential. The top electrode is 8.3 mm above the flat interface.

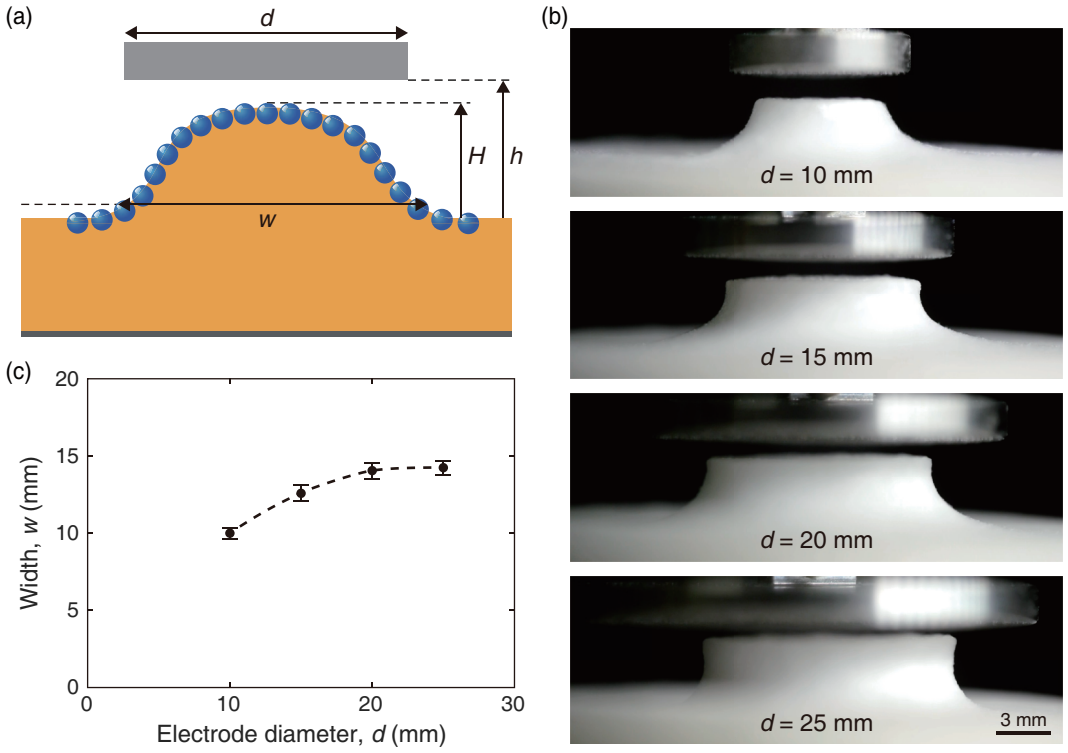


FIG. S3: Effects of electrode diameter on the width of upheaved raft. (a) Schematic of deformed particle raft at equilibrium state with varying top electrode diameter, $d$. (b) Upheaved rafts under top electrodes of different diameters. All experiments were conducted at $h = 3.8$ mm and $\phi = 10$ kV. (c) The width of the upheaved raft 0.5 mm above the unperturbed interface. Five experiments were conducted for each diameter.

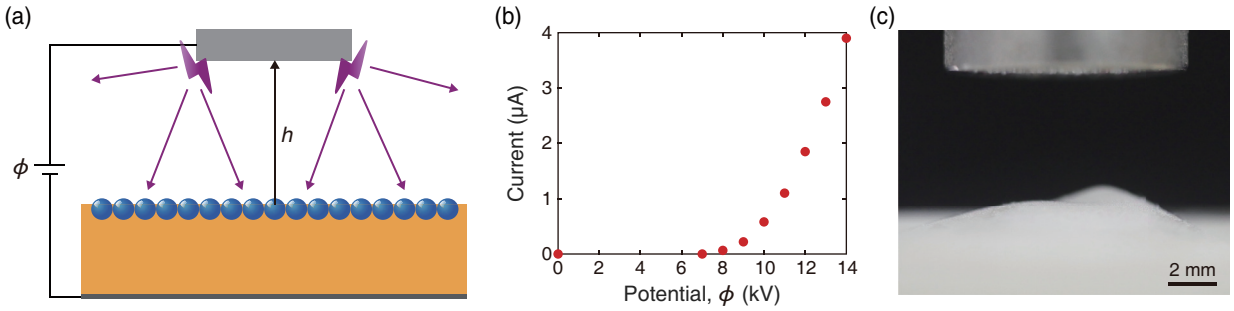


FIG. S4: Effects of electric breakdown under high electric potential. (a) Schematic of electric discharge near the top electrode when high $\phi$ is applied between two electrodes. (b) Experimentally measured electric current through the top electrode with different $\phi$. (c) Unstable particle raft due to electric discharge from the top electrode. The top electrode is at $h = 7$ mm, and $\phi = 13$ kV.

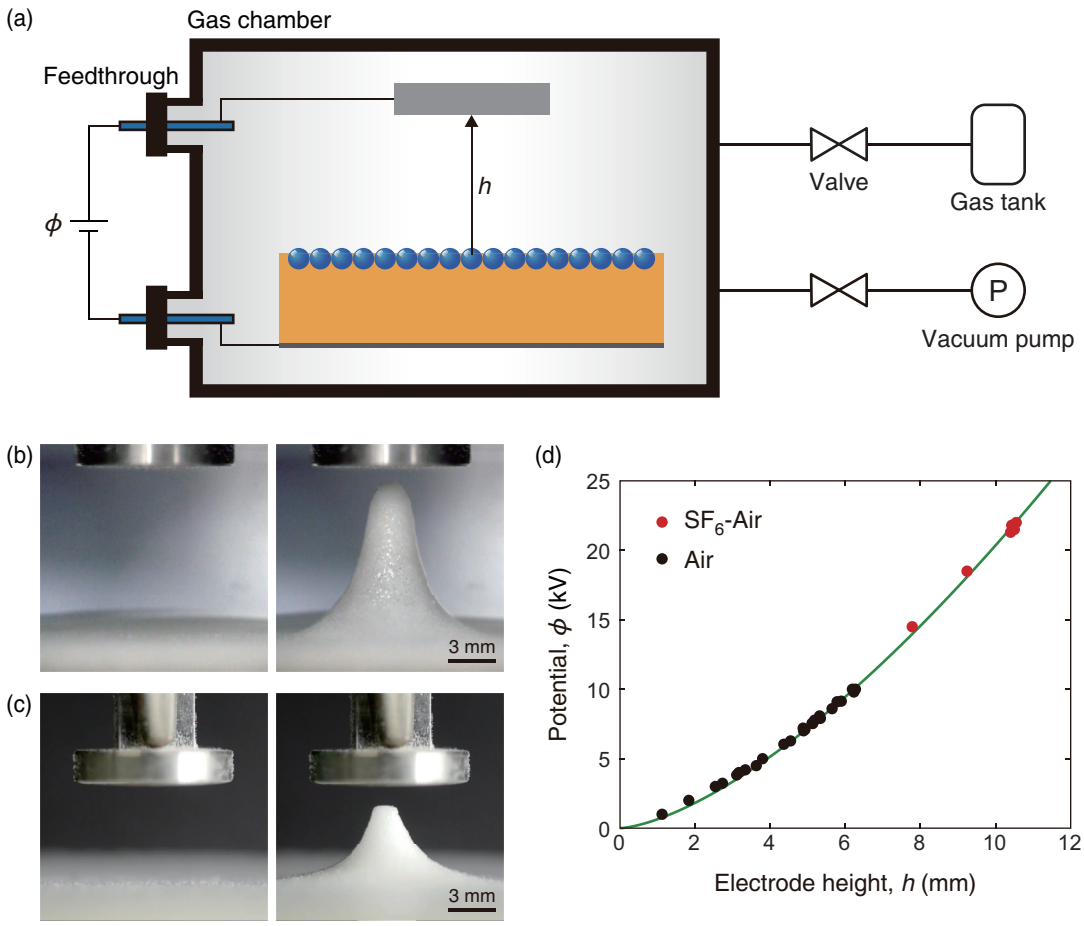


FIG. S5: Formation of a high-rise mound with increased electrode distance through gas substitution. (a) Schematic of the experimental setup for gas substitution. (b) Particle raft in the chamber filled with 1 bar of 10 vol.% air and 90 vol.% $SF_6$ with $h = 10.5$ mm and $\phi = 21.5$ kV. (c) Particle raft at atmospheric condition with $h = 6.4$ mm and $\phi = 10$ kV. (d) Circles correspond to the experimentally determined regime boundary where a strong uplift of particle raft occurs in atmospheric (black) and $SF_6$-rich (red) environments. The green line is plotted by our force-balance model, $\phi = \eta(\rho g/\Delta\epsilon)^{1/2}h^{3/2}$ with $\eta = 1.2$.

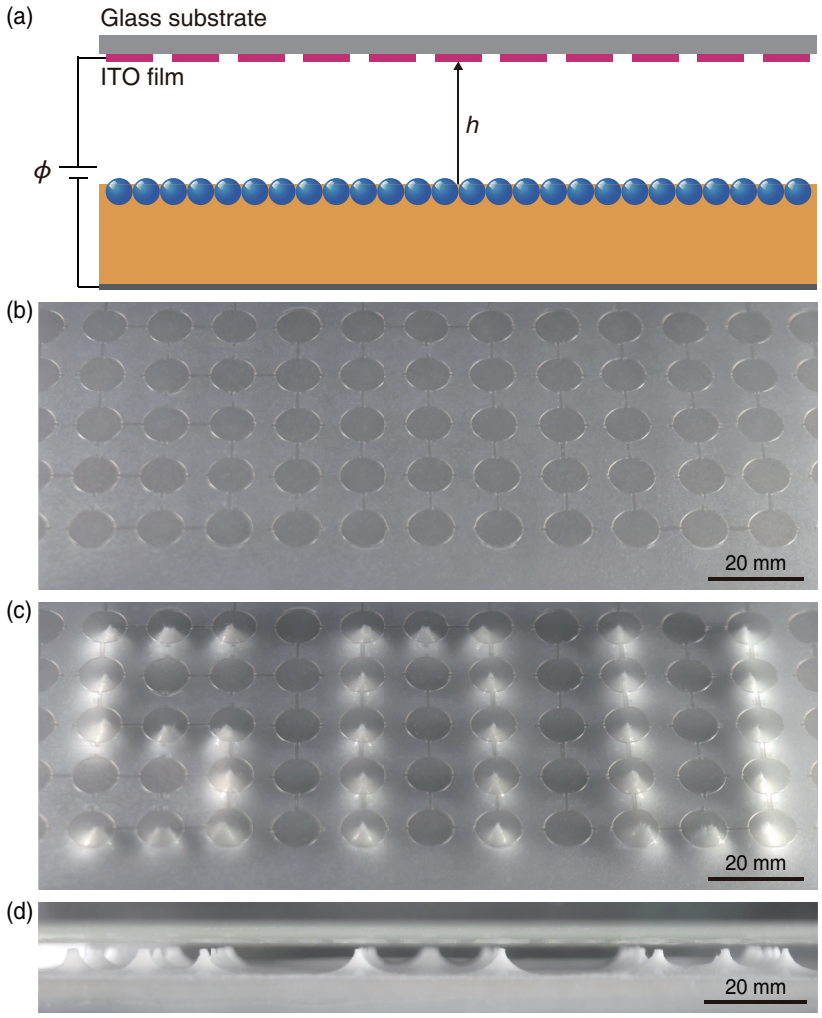


FIG. S6: Demonstrating the three-dimensional physical display using multiple electrodes. (a) Schematic of the experiment setup employing a polyethylene terephthalate (PET) film coated with an array of multiple electrodes of transparent ITO, which is attached to a glass plate for mechanical support. The electric potential of each electrode is controlled independently. (b) A tilted view of the initially flat particle raft with no electric field.(c) The 3D letters, SNU, are generated when the pertinent electrodes are turned on with $\phi = 10$ kV and $h = 6.5$ mm. (d) A side view of the 3D letters shown in (c).

## DESCRIPTION OF THE VIDEOS

**Movie S1: Fundamental modes in electro-morphing of particle rafts** - Fundamental morphing modes, i.e., upheaving, remote pulling, and horizontal translation. The electric potential difference is 10 kV in each experiment. The video plays at real-time speed.

**Movie S2: Shape control of a particle raft mound** - Various shape control schemes of a particle raft mound. (A) elongation by remote pulsing, (B) widening and pulling, (C) use of a large electrode, (D) enhanced upheaving in SF6-air mixture atmosphere, and (E) bare finger-driven morphing. The electric potential difference is 10 kV in (A-C), 21.5 kV in (D), and 12 kV in (E). The video plays at real-time speed.

**Movie S3: Multi-electrode system for human-machine interface and 3D physical display** - Feasibility of electro-morphing as a human-machine interface (A) and three-dimensional physical display (B) by using multiple fingers and conductive electrodes, respectively. In the physical display, the top plate is transparent as comprising an array of ITO electrodes. The electric potential difference is 10 kV in both experiments, and ITO electrodes are 6.5 mm above the unperturbed interface. The video plays at real-time speed.

# References

[1] W. Hertz, H. Motschmann and H. Wittel, *Proceedings of the IEEE*, 1971, **59**, 485-492.